A Dual-Pronged Solution for Accurate Decentralized Tag Systems: RSSD-Based DoA and Tag Design

Myoungsun Kim, *Graduate Student Member, IEEE*, Sirous Bahrami, *Senior Member, IEEE*, and Wonbin Hong, *Fellow, IEEE*

***Abstract*—Localization systems play a crucial role in various Internet of Things (IoT) applications; however, traditional techniques require significant computational resources and complex hardware, making them impractical for resource-limited devices. This article introduces a dual-pronged approach that addresses these challenges by focusing on reducing computational complexity, optimizing tag design, and enhancing Direction-of-Arrival (DoA) estimation accuracy in real-world scenarios. A received signal strength difference (RSSD)-based DoA method using a tilted array configuration is proposed, requiring only a single subtraction for RSSD calculation. A calibration technique mitigates anchor-tag misalignment, reducing root-mean-square error (RMSE) from 12.5° to 6°. Furthermore, antenna directivity and tilting angle are analyzed, introducing RSSD slope as a metric for design-performance optimization. Experiments confirm that higher RSSD slopes improve estimation accuracy and noise robustness. These findings enable efficient localization solutions for small, power-constrained devices, paving the way for real-world IoT applications.**

***Index Terms*—Mobile antenna, received signal strength (RSS)-based Direction-of-Arrival (DoA) (RSS-based DoA), ultra-wideband (UWB) localization.**

I. Introduction

As Internet of Things (IoT)-based localization technologies continue to rapidly advance, they are evolving toward integrating spatial information into IoT data, enabling autonomous position recognition without human intervention [1]. Consequently, localization technologies that have been successfully commercialized in military, construction, and industrial machinery applications are now expanding into various IoT applications [2], including smart homes [3], logistics [4], emergency services, and environmental monitoring.

A primary approach to localization in IoT environments is the use of the global navigation satellite system (GNSS). However, many IoT devices face challenges in receiving GNSS signals due to cost constraints and power consumption limitations [5]. Additionally, alternative localization methods utilizing environmental sensors that are embedded in common IoT devices, such as magnetometers, barometers, light sensors, and sound sensors, have been explored. While these sensors provide useful data, they are typically designed to be low-cost, leading to significant measurement errors. Furthermore, they are highly susceptible to external environmental factors, such as temperature fluctuations, humidity variations, and electromagnetic interference [6].

Wireless signal-based localization techniques have been proposed, including ultrawideband (UWB), Wi-Fi [7], Bluetooth low energy (BLE), long range wide-area network (LoRaWAN), and narrowband IoT (NB-IoT) [8]. These methods estimate position by leveraging various signal characteristics. Among the most widely used signal metrics for localization are Time-of-Arrival (ToA), channel state information (CSI), and received signal strength (RSS). ToA and CSI-based localization systems achieve high localization accuracy [1]. However, ToA requires precise clock synchronization, which resource-limited devices cannot support, while CSI-based methods are constrained by equipment capabilities and computational complexity. In contrast, RSS-based localization relies solely on RSS, making it a cost-effective and easy-to-implement solution. However, this simplicity comes at the expense of reduced accuracy, as RSS measurements are highly susceptible to environmental factors, including multipath effects.

To improve localization accuracy, RSS-based Direction-of-Arrival (DoA) (RSS-based DoA) estimation methods have been suggested [9], [10], [11], utilizing the relative RSS values between antennas. The system can enhance DoA estimation accuracy by reducing the impact of signal fluctuations and improving robustness against external interference. Traditional RSS-based DoA methods rely on centralized systems with multiple antennas, often requiring bulky hardware and complex signal processing, making them unsuitable for handheld and decentralized tag devices.

In direct response to these limitations, we propose a lightweight RSS difference (RSSD)-based method that simplifies hardware requirements while maintaining accurate DoA estimation. Our contributions include the following.

1) *An Ultralow-Complexity Core Computation:* We propose an RSSD-based DoA estimation method whose core operation involves only a single subtraction. This

Received 12 February 2025; revised 4 August 2025 and 21 August 2025; accepted 25 August 2025. Date of publication 29 August 2025; date of current version 7 November 2025. This work was supported in part by the Government through the Ministry of Science and Technology Information and Communication, and in part by the National Research Foundation of Korea (NRF) under Grant RS-2025-00514623. *(Corresponding author: Wonbin Hong.)*

The authors are with the Department of Electrical Engineering, Pohang University of Science and Technology, Pohang 37673, Republic of Korea (e-mail: myoungsunkim@postech.ac.kr; bahramis@postech.ac.kr; whong@postech.ac.kr).

Digital Object Identifier 10.1109/JIOT.2025.3604049

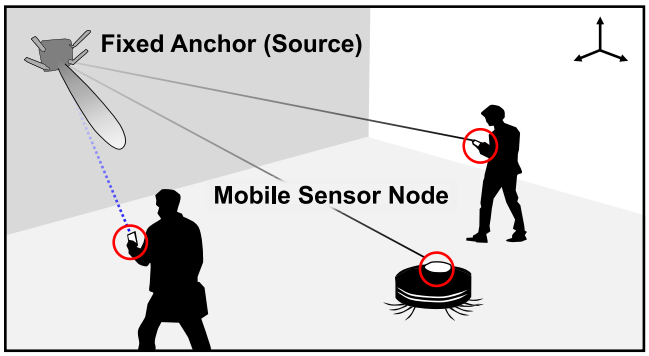

Fig. 1. Real-world scenario demonstrating decentralized localization system using the RSSD-Based DoA Method within a confined region utilizing mobile sensors.

enables a theoretical time complexity of O(1)—orders of magnitude lower than existing Angle-of-Arrival (AoA) methods based on covariance matrix analysis.

2) *A Practical Orientation Calibration Method:* We introduce a lightweight yet effective calibration technique that explicitly separates dynamic orientation offsets from dynamic incident angle estimation. This calibration allows the method to remain robust in real-world mobile scenarios without relying on active alignment mechanisms.
3) *A Novel Design Metric—RSSD Slope:* We introduce RSSD slope as a novel quantitative metric for characterizing and optimizing tag antenna design. By evaluating tag variations across different tilt angles and antenna directivities, the RSSD slope effectively captures the tradeoff between angular sensitivity and estimation coverage. This metric provides a practical design tool for system developers, enabling systematic and data-driven optimization of hardware configurations—an aspect that has been largely overlooked in prior RSS-based DoA studies.

The proposed dual-pronged approach synergistically integrates a computationally efficient algorithm with a practical hardware design methodology. By tackling both software and hardware aspects in synergy, our solution offers a holistic framework optimized for real-world decentralized systems. This approach moves beyond advocating for algorithmic superiority alone and presents a comprehensive solution that is both novel and practical. To validate the effectiveness and robustness of this approach, we conducted a comprehensive set of experiments in diverse environments. First, in a controlled anechoic chamber, we systematically analyze the impact of key antenna design parameters—namely, directivity and tilt angle—on DoA estimation accuracy under varying noise conditions. Subsequently, to demonstrate real-world viability, we perform experiments outside the anechoic chamber, validating the system's performance and the efficacy of our calibration method across various tag distances and orientations. The results demonstrate that this approach is highly effective and well-suited for decentralized systems where nodes must operate independently and efficiently.

This article is organized as follows. Section II reviews related works to contextualize and clarify the contributions of this study. Section III establishes the theoretical background of the proposed RSSD-based DoA estimation and introduces a novel calibration method designed to address tag mobility and orientation variations. Section IV presents the experimental validation of the proposed framework, including a quantitative comparison with existing approaches. Section V provides an in-depth analysis of key antenna design factors, such as directivity and tilting angle, and introduces the "RSSD" slope as a new metric for optimizing the tradeoff between tag design and DoA estimation accuracy. Section VI discusses the study's limitations and outlines promising directions for future research. Finally, Section VII concludes this article by summarizing the key findings.

II. Related Work

A. Ultralow-Complexity Core Computation

As illustrated in Fig. 1, the localization system consists of nodes and anchors [1], [12], [13]. Nodes represent compact handheld devices, such as mobile phones or smart tags, while anchors serve as fixed reference points, typically equipped with powerful hardware to support high-accuracy computations. As established in the introduction, decentralized systems offer enhanced robustness and privacy [1], [14]. However, this autonomy poses significant challenges for resource-constrained nodes [15].

Conventional time-domain methods [16], which estimate range based on Time-of-Flight (ToF) or Time Difference of Arrival (TDoA), face significant scalability limitations, as they require strict time synchronization and increased hardware complexity when scaling to a large number of nodes. AoA-based techniques, such as multiple signal classification (MUSIC), have been widely employed due to their high angular resolution. MUSIC relies on covariance matrix calculation and eigenvalue decomposition, with computational complexity typically around $O(M^3+M^2N)$ [17], [18], where M denotes the number of sensors and N the number of snapshots. Similarly, the estimation of signal parameters via rotational invariance techniques (ESPRIT) algorithm [17], although avoiding exhaustive spectral searches, still necessitates singular value decomposition and thus maintains a computational complexity on the order of $O(M^3)$. Such algorithms, as pointed out in [17] and [18], become impractical for real-time or resource-constrained applications unless deliberate efforts are made to reduce computational burden [19]. Addressing these challenges, we propose a RSSD-based DoA estimation approach, whose core operation requires only a single subtraction. This dramatically reduces theoretical time complexity to O(1), significantly below that of conventional high-resolution methods, such as MUSIC or ESPRIT, which rely heavily on matrix operations. This minimal computational requirement makes the proposed RSSD method particularly advantageous for mobile or energy-sensitive devices.

B. Practical Orientation Calibration Method

While anchor position calibration is well-studied, orientation calibration—a critical factor for DoA estimation accuracy—has been largely overlooked in decentralized systems. Anchor orientation directly influences system

performance through two critical factors [20]. First, practical UWB antennas deviate from ideal omnidirectional behavior and exhibit unique radiation patterns. These patterns cause directional variations in RSS depending on the relative orientation between the anchor and the tag [12], [13], [20]. Second, misoriented antennas can distort or attenuate received signals, leading to subtle ToF measurement errors. These accumulate into systematic ranging biases and degrade localization performance even under nominal conditions [13], [20].

The impact of anchor orientation becomes more critical in DoA estimation systems that use multiple antennas, where performance heavily depends on accurate antenna response modeling [13]. However, antenna patterns characterized under ideal laboratory conditions often diverge from their behavior in real deployments—such as wall-mounted or mobile platforms—due to physical misalignment and environmental coupling [12]. This model mismatch impairs directional reliability by distorting the actual antenna response used for angular inference. Simulation and theoretical studies confirm that such mismatches can raise DoA root-mean-square error (RMSE) by several degrees, and in some cases up to 10°, especially under limited SNR and snapshot conditions [21]. These results underscore the need for practical, lightweight orientation-aware calibration methods tailored for real-world deployments.

To address this issue, recent work has proposed the simultaneous localization and calibration (SLAC) framework [22], which jointly corrects antenna response errors and ranging biases in real time. SLAC continuously updates the antenna response model using measurements from multiple incident angles, effectively compensating for orientation-induced artifacts. Experimental results validate its effectiveness in improving localization accuracy under realistic deployment conditions.

While orientation calibration has been widely studied in centralized localization systems [23], decentralized RSS-based DoA systems have largely overlooked the effects of anchor-tag misalignment. In particular, RSSD-based DoA methods, which infer incident angles from RSSDs, are especially sensitive to antenna radiation patterns [20]. Misalignment between the anchor's assumed and actual orientation can thus introduce substantial estimation errors, yet this factor remains underexplored. Although some prior works have observed accuracy degradation due to orientation errors [24], they have not investigated the underlying causes or proposed real-time corrective strategies. For instance, in [24], an RSS-based DoA system using a rat-race coupler and two patch antennas demonstrated improved performance through manual orientation adjustment. However, the effects of orientation misalignment were neither systematically analyzed nor addressed through automated calibration.

To overcome these limitations, we introduce a lightweight yet effective orientation calibration method designed to decouple dynamic orientation offsets from incident angle estimation. This calibration framework does not rely on any active mechanical alignment mechanism and remains robust under real-world mobile conditions. By adopting a closed-form model that jointly accounts for both tag orientation and incident angle variation, the proposed method provides a practical and scalable solution for decentralized localization systems employing RSSD-based DoA estimation.

C. Novel Design Metric—RSSD Slope

Antenna design is a critical yet often overlooked aspect in optimizing RSS-based DoA systems, especially under the strict form-factor constraints of IoT devices [25]. While conventional multielement antenna arrays require about a half-wavelength element spacing to ensure high accuracy, this spatial requirement becomes a significant limitation in IoT applications where device size is constrained [19]. To overcome these constraints, recent research efforts have explored novel methods utilizing single or minimal antenna elements. For instance, frequency scanning antennas (FSA) leverage frequency-dependent beam steering characteristics [26], [27]. When an IoT device equipped with a single antenna scans signals across different frequency channels—such as Wi-Fi probe signals—the direction of the strongest received frequency channel can provide a reliable estimate of the incoming signal's angle. This method enables precise direction-finding and localization capabilities in low-cost IoT devices without additional complex hardware.

However, despite various methodological advancements, there has been insufficient discussion regarding explicit antenna design optimization. It is crucial to consider practical constraints, particularly limited physical space, when designing antennas aimed at achieving higher localization accuracy, [28], [29]. Under strict size constraints, a simpler system that meets operational needs is often preferable to a complex one with only marginally higher precision [30].

To systematically address this challenge, we introduce the RSSD slope as a novel quantitative metric for characterizing and optimizing tag antenna design, explicitly taking into account the physical size and form-factor constraints of IoT devices. The RSSD slope evaluates variations in the RSSD across various antenna tilt angles and directivities. Consequently, this metric offers a practical and data-driven tool for hardware designers and system developers, facilitating optimized antenna configurations. Prior studies focusing on RSS-based DoA estimation have largely neglected such antenna-centric design optimization metrics; thus, our proposed RSSD slope fills a critical research gap and provides a structured framework for improving localization accuracy within realistic IoT constraints.

III. RSSD-Based DoA Estimation Method

To enable decentralized localization [31], our system adopts a minimal configuration consisting of a single anchor and a single mobile tag, as illustrated in Fig. 2(a). In this setup, the tag is equipped with two spatially separated antennas, forming a compact receiver array. Unlike conventional uniform arrays, the two antennas are tilted at a predefined angle α to deliberately induce an angular asymmetry in reception characteristics, as shown in Fig. 3. This tilted array configuration plays a crucial role in enabling DoA estimation using RSSD. As the incident signal angle varies, the directional gain profiles of the tilted antennas result in systematic differences in received

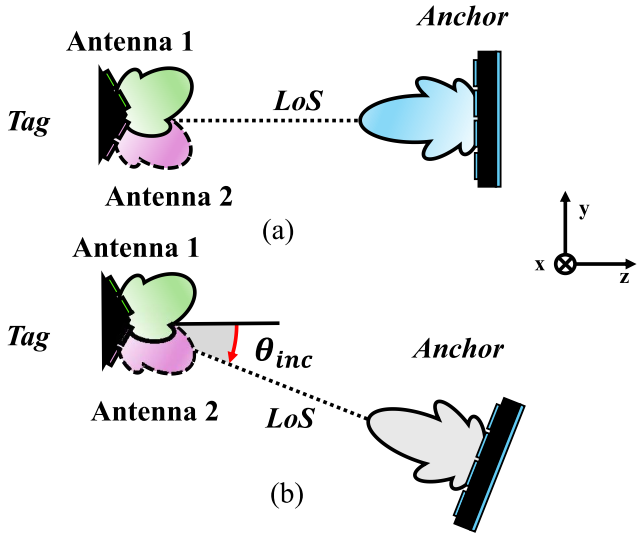

Fig. 2. Schematic of anchor and tag configuration for Incident angle θ_{inc}: Anchor oriented toward the tag.

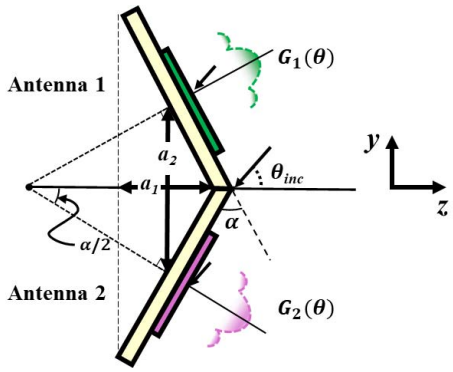

Fig. 3. Tilted antenna array tilted at an angle α receives an incoming signal from an incident angle θ_{inc}. (for a tilted array configuration consisting of 1×2 patch arrays tilted at 60°, $a_1 = 50$ mm, $a_2 = 87$mm)

power, creating an RSSD signature that is uniquely correlated with the incident angle. Under ideal conditions—where the anchor and tag are fixed and well-aligned, this angular correlation allows precise DoA estimation, as illustrated in Fig. 2(b).

However, real-world conditions deviate significantly from this idealized scenario. In practical deployments, the tag may experience arbitrary mobility and orientation changes. Such variations cause a misalignment between the anchor-to-tag direction and the tag's antenna frame, which distorts the RSSD measurements and degrades estimation accuracy. To make RSSD-based DoA estimation viable in mobile settings, it is essential to account for these deviations and compensate for them. To address this challenge, this section proceeds in two stages. Section III-A presents an analytical model for ideal RSSD-based DoA estimation assuming perfect alignment.

Section III-B then extends the model to incorporate misalignment effects and proposes a lightweight calibration method to enhance estimation robustness in mobile scenarios.

A. Analytical Model of Proposed RSSD-Based DoA Method

Consider two ideal alignment scenarios where the anchor faces the tag. In Fig. 2(a), the anchor and tag are aligned along

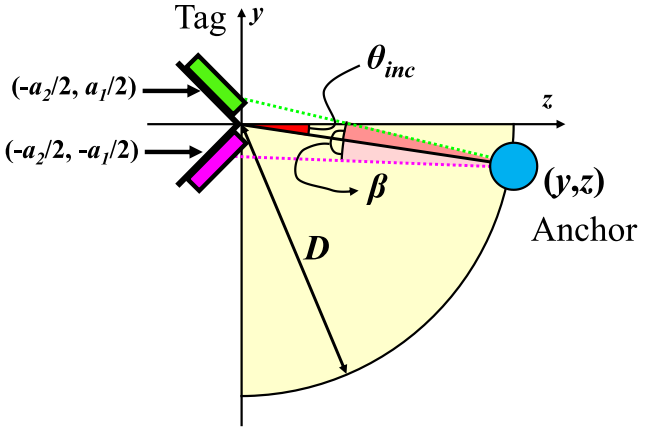

Fig. 4. Schematic illustrating the center displacement effect on channel gain and anchor gain variation. Similar to Fig. 3, Antenna 1 is depicted in green, while Antenna 2 is shown in pink. Setting the center edge of the tilted array as (0,0), the centers of the tag antennas are represented as $(-a_1/2,\ a_2/2)$ and $(-a_1/2,\ -a_2/2)$, respectively.

a Line-of-Sight (LoS) at a fixed distance D. Fig. 2(b) depicts the tag or anchor rotating around the other while maintaining distance D, with the anchor always oriented toward the tag. With fixed coordinates referenced to the tag's symmetry axis, the incident angle, θ_{inc}, in the elevation plane is defined as the angle between the LoS path and the z-axis in the elevation plane. The proposed DoA method is based on the ratio of RSS between two tilted antennas, defined as RSSD in logarithmic form. Thus, the proposed method only requires a single subtraction calculation of the RSS, providing the simplest computation for a DoA system

$$\text{RSSD} \triangleq \text{RSS}_1^{\text{dB}} - \text{RSS}_2^{\text{dB}}. \tag{1}$$

In (1), RSS_1 and RSS_2 denote the RSSs at Antenna 1 and Antenna 2, as shown in Figs. 2 and 3, respectively. Under the unobstructed LoS propagation assumption, as described in [32], RSS of each nth antenna can be denoted as

$$\text{RSS}_n^{\text{dB}}(\theta_{\text{inc}},\ D) = G_n^{\text{dB}}(\theta_{\text{inc}}) + P_n(D) + w_n \tag{2}$$

where G_n^{dB} represents the nth antenna gain pattern, $P_n(D)$ is the incident power at the receiver and w_n denotes the noise of the radio channel and receiver. Incident power P_n can be expressed as

$$\text{P}_n(D) = P_T + \boldsymbol{A} \cdot 10\log\left(\frac{4\pi D_n}{\lambda}\right) + G_T^{\text{dB}} \tag{3}$$

where P_T and G_T^{dB} are the anchor transmitted power and gain, respectively. Also, the channel gain is expressed based on the distance between anchor and the nth receiver D_n as

$$D_n = \sqrt{D^2 + \left(\text{D}\sin\ \theta_{\text{inc}} + (-1)^{n-1}\frac{a_2}{2}\right)^2}. \tag{4}$$

Due to the tilted array configuration, the phase center of each antenna is offset by $a_2/2$ from the center of the array along the y-axis, as illustrated in Figs. 3 and 4. Here, a_1 and a_2 denote the spatial separation between the tag antennas in the z- and y-directions, respectively, in the tilted array configuration. This phase-center offset causes each antenna to experience a different channel gain, as illustrated in dotted

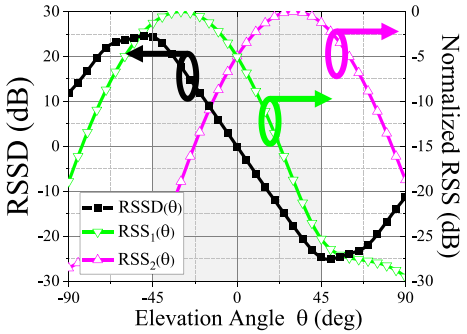

Fig. 5. Normalized radiation pattern and RSSD pattern using 1 × 2 array antennas tilted at 60 °. Green scattered line represents for RSS pattern for Antenna 1 and pink for Antenna 2. The shaded region representing monotonically decreasing region in RSSD pattern is denoted as the FoV.

lines in Fig. 4. However, under the far-field condition and certain approximations, where the tag distance a_2 is much smaller than the LoS path length (D), the range variation of distance ratio (D_1/D_2) can be simplified and determined as

$$1 - \frac{a_2}{2D} \leq \frac{D_1}{D_2} \leq 1 + \frac{a_2}{2D}. \tag{5}$$

These distance variations are negligible and can therefore be omitted from the overall RSSD calculation for simplification. Furthermore, as the distance between the anchor and the tag increases, the channel gain variations diminish further. For instance, when the distance between tag antennas a_2 is set to 87 mm and the anchor-tag distance D is 3000 mm, the channel gain exhibits minor variations ranging from −0.13 to 0.13 dB.

Although the received power follows a stochastic variation due to fading and noise, averaging multiple RSS measurements reduces the effect of noise, allowing the mean value to be used for estimation. Therefore, to establish the reference RSSD as a function of incident angle θ_{inc}, the noise component w_n in (2) is neglected. Additionally, if the tag's two antennas are identical, each antenna's gain pattern G_n can be approximated by a common pattern G_0 which is oriented toward z-axis and tilting angle α. Consequently, the RSSD expression can be simplified and recast as

$$\begin{aligned} &\text{RSSD}\ (\theta_{\text{inc}}) = G_1^{\text{dB}}(\theta_{\text{inc}}) - G_2^{\text{dB}}(\theta_{\text{inc}}) \\ &= G_0^{\text{dB}}\left(\theta_{\text{inc}} + \frac{\alpha}{2}\right) - G_0^{\text{dB}}\left(\theta_{\text{inc}} - \frac{\alpha}{2}\right) \triangleq \ \text{RSS}D_{\text{tag}}(\theta_{\text{inc}}). \end{aligned} \tag{6}$$

Equation (6) shows that for a fixed tilting angle, the incident angle is the only variable influencing the expected RSSD. Fig. 5 helps illustrate the derivation of $RSSD(\theta)$ derivation, showing the normalized RSS patterns of antenna 1 and antenna 2. The channel gain variation due to mismatched phase centers is not reflected. The simulation results shown in Fig. 5 are based on identical tag antennas, specifically a 1 × 2 patch antenna array, as introduced in Section V-A, with a tilt angle of 60°. The normalized pattern of each antenna is demonstrated in green and pink, similar to Fig. 3, while RSSD(θ) is in black. Hence, there is a one-to-one correspondence between the RSSD level and the incident angle.

Consequently, the estimated incident angle $\widehat{\theta}$ can be obtained by minimizing an error function

$$\widehat{\theta} = \text{argmin}_{\theta_{\text{inc}}} \mid \text{RSSD}(\theta_{\text{inc}}) - \text{RSS}D_m \mid \tag{7}$$

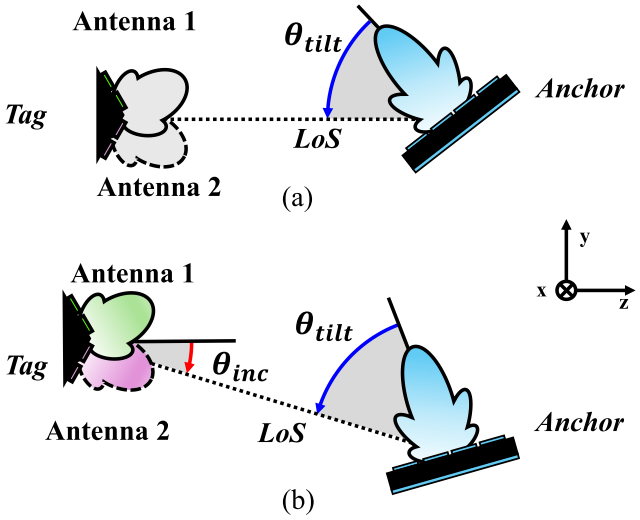

Fig. 6. Schematics of Anchor Misalignment Variation in a Tilted Array Configuration: (a) $\theta_{\text{inc}} = 0°$, (b) $\theta_{\text{inc}} \neq 0°$.

where RSSD(θ) defined as in (6), and RSSD_m is the measured RSSD value. This estimation approach simplifies the estimation process, making it more robust against experimental outliers compared to methods that rely on complex distributional assumptions.

In this article, the Field-of-View (FoV) is defined as the range where RSSD(θ) monotonically increases or decreases and includes an incident angle of 0° [20]. As shown in Fig. 5, the shaded regions representing the monotonically decreasing areas correspond to the FoV. The FoV ensures a one-to-one correspondence between the incident angle and RSSD(θ) by constraining the estimable angular range, allowing a specific RSSD value to uniquely determine a single incident angle.

B. Calibrating Tag Misalignment in Real-World Scenarios

The previous section and related studies primarily assume an ideal scenario in which the anchor remains continuously oriented toward the tag. However, in real-world operation, the tag not only moves but also rotates, causing the incident angle and the tag's orientation to vary over time. In the scenario where $\theta_{\text{inc}} = 0°$ in Fig. 6(a), the tag is oriented directly toward the anchor, resulting in an incident angle of effectively 0°. According to (6), the RSSD value should be zero in this case. However, in practice, the measured RSSD value deviates from zero. This discrepancy arises because the RSSD definition in (6) assumes that the anchor continuously faces the tag, as shown in Fig. 2(b).

Considering the general scenarios involving the characteristics of a mobile tag, Fig. 6(b) illustrates a situation where the anchor and tag orientations are misaligned. As shown in Fig. 6, the angle θ_{tilt} is introduced to quantify this misalignment between the anchor and the tag. Consequently, the RSSD definition needs to be updated to account for the combined effects of orientation variation and incident angle, providing a more accurate representation of real-world conditions.

As mentioned earlier, the LoS path, which determines the incident angle, is defined as the path connecting the anchor to

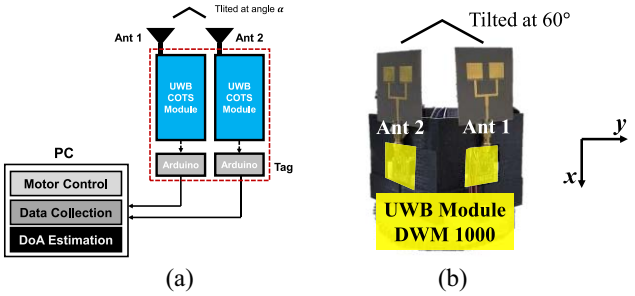

Fig. 7. (a) Schematic and (b) photograph of the tag module used to validate the proposed method.

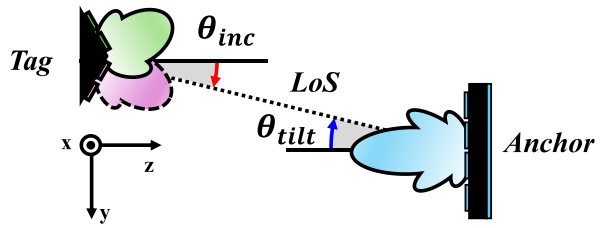

Fig. 8. Schematic of face-to-face orientation suggesting the special relationship between θ_{tilt} and θ_{inc}.

the center of the tag, as shown in Fig. 3. Each antenna is offset from the tag's center, which causes a center-displacement effect on both the anchor gain and the channel gain. As shown earlier, the difference in channel gain due to this offset can be neglected. However, anchor gain variation which results from the angular shift, indicated by the angles colored in pink in Fig. 4, in the transmitting power pattern cannot be ignored [33]. This angular shift, which is a function of the tag geometry and the distance (D), introduces an effective offset in the anchor's perceived angle. Under far-field conditions where D is large, this offset can be approximated as an effective angular constant, denoted here as β, for a given tag hardware configuration.

Equation (8) gives the incident power at the nth receiving antenna, where the transmit antenna gain term is $G_{T,n}(\theta_{\text{tilt}})$ instead of G_T. The transmitted gain pattern $G_{T,n}$ varies with the anchor orientation variation θ_{tilt}. An angular offset β is introduced to account for this misalignment in the transmit gain. Assuming the tag's two antennas are symmetric about the tag's center (pointing in opposite directions), each antenna's gain pattern is shifted by $+\beta$ or $-\beta$

$$P_n(D,\theta_{\text{tilt}}) = P_T + \boldsymbol{A}\cdot 10\log\left(\frac{4\pi D_n}{\lambda}\right) + G_{T,n}(\theta_{\text{tilt}}) \quad (8)$$

$$G_{T,n}(\theta_{\text{tilt}}) \cong G_T(\theta_{\text{tilt}} + (-1)^n\beta)). \quad (9)$$

As a result, as depicted in Fig. 6(a), the variation of RSSD with respect to the anchor orientation θ_{tilt} can be derived as in

$$\begin{aligned}\text{RSSD}\ (\theta_{\text{tilt}}) &= G^{\text{dB}}_{T,1}(\theta_{\text{tilt}}) - G^{\text{dB}}_{T,2}(\theta_{\text{tilt}})\\ &= G^{\text{dB}}_T(\theta_{\text{tilt}} - \beta) - G^{\text{dB}}_T(\theta_{\text{tilt}} + \beta) \triangleq \text{RSSD}_{\text{anc}}(\theta_{\text{tilt}}).\end{aligned} \quad (10)$$

Finally, real-world applications, as shown in Fig. 6(b), require considering both effects of incident angle and orientation variation. As a result, the general solution for real-world application can be represented as a summation of RSSD_{tag} and RSSD_{anc} in

$$\begin{aligned}\text{RSSD}\ (\theta_{\text{inc}},\theta_{\text{tilt}}) &= G^{\text{dB}}_0\left(\theta_{\text{inc}} + \frac{\alpha}{2}\right) - G^{\text{dB}}_0\left(\theta_{\text{inc}} - \frac{\alpha}{2}\right)\\ &\quad + G^{dB}_T(\theta_{\text{tilt}} - \beta) - G^{dB}_T(\theta_{\text{tilt}} + \beta)\\ &\triangleq RSSD_{\text{tag}}\ (\theta_{\text{inc}}) + RSSD_{\text{anc}}\ (\theta_{\text{tilt}})\end{aligned} \quad (11)$$

Here, RSSD_{tag} represents the effect of incident angle, while RSSD_{anc} accounts for the anchor orientation, defined in (6) and (10), respectively. The key to decoupling, as shown in (11), lies in the fact that the incident angle θ_{inc} and tag orientation θ_{tilt} are geometrically independent variables that affect different terms in the link budget. θ_{inc} primarily governs the receiving antenna gain G_r at the tag, while θ_{tilt} primarily affects the transmitting antenna gain G_t as seen by the tag's displaced antennas. Because these are independent angular effects, their contributions to the final RSSD are separable and additive in the logarithmic domain. By incorporating both incident angle and orientation variation effects, the proposed calibration approach in (11) provides a practical, computationally efficient correction to traditional RSS-based DoA estimation. Unlike prior work that assumes fixed orientation, this model adapts dynamically to real-world mobility conditions. The proposed calibration method enhances DoA estimation accuracy without introducing a complex process, validating its effectiveness as demonstrated in Section IV.

IV. Experimental Validation of Proposed Method

A. Experimental Setup

To verify the applicability and validity of the proposed method in real-world, experiments are conducted. Each tag and anchor consists of UWB commercial off-the-shelf (COTS) modules [34], antennas, and a microcontroller board. Fig. 7(a) shows a schematic of the tag device, and Fig. 7(b) provides a photograph of the implemented tag. The tag device with a 1 × 2 array antenna and a tilting angle of 60° is used, depicted in Fig. 7(b). The 60° tilt angle is selected through a systematic design space exploration, as described in Section V. The anchor consists of a 1 × 4 array antenna and transmits a packet every second. The tag collects the transmitted packets for one minute and estimates the incident angle based on the mean received power.

Theoretically, the proposed method can be applied to any scenario with varying anchor orientations. Therefore, a general face-to-face orientation is selected to replicate real-world scenarios. In this face-to-face setup, the anchor and tag are positioned facing each other, as shown in Fig. 8. In the face-to-face setup, θ_{tilt} and θ_{inc} in (11) have a special relationship, where they are equivalent in magnitude but have opposite signs, as shown in Fig. 8. Therefore, with a single variable θ_{inc}, the final equation in (11) can be rewritten in

$$\text{RSSD}(\theta_{\text{inc}})(\text{dB}) = RSSD_{\text{tag}}(\theta_{\text{inc}}) + RSSD_{\text{anc}}(-\theta_{\text{inc}}). \quad (12)$$

Since the total RSSD(θ) is influenced by both the tag and the anchor, it is essential to separately characterize the contributions of RSSD_{tag} and RSSD_{anc} before applying the calibration method. The extracted values from controlled

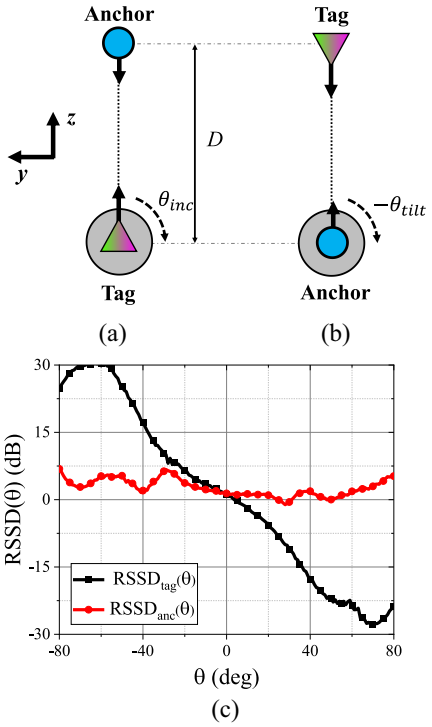

Fig. 9. (a) Schematic setting for measuring the effect of incident angle variation and (b) anchor orientation. (c) Measurement results of the angle variation illustrated in Fig. 9(a) and (b).

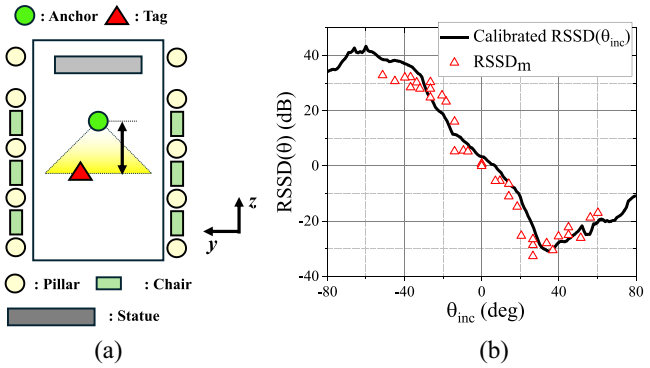

Fig. 10. (a) Schematic of Experimental setup for verifying proposed calibration method outside the anechoic chamber. The overall size of the experimental space, outlined by the black solid line, is defined as 11.7 m × 19.8 m. (b) Comparison between calibrated reference *RSSD* and Measured *RSSD* in a face-to-face orientation.

TABLE I
RMSE COMPARISON (CALIBRATION VERSUS NO CALIBRATION)

Estimation Error	Without Calibration	With Proposed Calibration
RMSE (°)	12.5	6.0

scenarios, as shown in Figs. 2(b) and 6(a), allow us to refine the final calibration equation (12). Accordingly, to replicate these controlled scenarios, the schematics of the experimental setups for obtaining RSSD$_{tag}$ and RSSD$_{anc}$ are constructed, as illustrated in Fig. 9(a) and (b), respectively. In this setup for RSSD extraction, the distance (D) between anchor and tag is set to 3.6 m. Fig. 9(c) presents the measurement results as a function of the rotating angle θ_{inc} or θ_{tilt}, where the black line represents RSSD$_{tag}$ and the red line represents RSSD$_{anc}$

B. Validation Outside the Anechoic Chamber

The experimental setup for verification of the face-to-face scenario is illustrated in Fig. 10(a). Validation experiments are conducted within a space measuring 11.7 by 19.8 m in the yz plane. The area contained eight pillars, six chairs, and a statue distributed within the experimental space. In real-world localization scenarios, the distance between the tag and anchor is variable and cannot be fixed. As the anchor-tag distance increases, multipath effects and power attenuation become more pronounced. Unlike previous studies that validate DoA estimation at a fixed calibration distance [27], this work verifies the approach's validity under various anchor-tag distances by maintaining a face-to-face orientation, as shown in Fig. 10(a), while moving the tag in both the y and z directions.

The moving step along the y-axis is set to 45 cm, which is the same as the floor tile's width. The tag moves along the y-axis within the following ranges: from -2.7 to 2.25 m at $z = -1.8$ m, from -2.7 to 2.7 m at $z = -2.7$ m, and from -1.8 to 2.7 m at $z = -3.6$ m. The origin is set at the position of the reference point, which is the location of the anchor. By moving the tag in the yz plane relative to the anchor, the ground truth of incident angle is determined by the ratio of displacement in the y- and z-directions. Specifically, the ground-truth incident angle θ_{GT} is defined as

$$\theta_{\text{GT}} = \left(\frac{y}{z}\right). \tag{13}$$

In (13), y and z represent the displacement in the y- and z-directions, respectively, as well as the coordinates of the tag relative to the origin. Using the proposed model (12), we validated the proposed method by comparing the ground-truth angle θ_{GT} from (13) to the estimated angle $\widehat{\theta}$ from (7) computed with the calibrated RSSD from (12).

For evaluation, an average of over 60 packets was selected based on empirical tests. It is important to note that allocating a full minute for collection intervals naturally improves accuracy by mitigating environmental noise effects. However, a shorter averaging window can still yield high accuracy levels. Thus, for practical implementations where response speed or power efficiency is critical, shorter averaging intervals may represent an optimal balance between accuracy and resource utilization.

The mean value of RSSD$_m$ is used in (7). The RSSD$_m$ values with final RSSD(θ) are plotted in Fig. 10(b). Fig. 10(b) plots the calibrated reference RSSD curve represented as a black line against the measured RSSD$_m$ values from 36 test positions. Fig. 10(b) indicates a close alignment between the calibrated RSSD and RSSD$_{\text{m}}$.

To confirm the effectiveness of the proposed approach quantitatively, DoA estimation errors with and without calibration are derived and compared. The DoA estimation is conducted within the FoV range. The RMSE of the DoA estimation comparison is presented in Table I. Without calibration, using

TABLE II
COMPUTATIONAL COMPLEXITY AND HARDWARE REQUIREMENTS OF REPRESENTATIVE DOA METHODS

Method	Complexity	Principle	Processing Time*	HW Requirement
Proposed	O(1)	RSSD	1.53 s	2 antennas
Monopulse	O(1)	Sum/Diff.	2.23 s	≥2 antennas
MUSIC	$O(M^3+M^2N)$	Subspace (Eigen)	High	Cal. array** (M>2)
ESPRIT	$O(M^3)$	Subspace (Rot.)	High	Cal. array** (M>2)
RTT-based	O(1)	Round-trip Time	N/A	Precise clock + extra HW

* Processing time measured on MATLAB; MUSIC/ESPRIT significantly slower (>>100×), RTT depends mainly on hardware.
** Cal. array = calibrated multi-antenna array.
*** Precise clock + extra HW = high-accuracy synchronization and additional circuitry required for RTT.

a typical DoA estimation equation suggested in (6), the estimation error is 12.5°. However, after applying the calibrated RSSD considering the tag and anchor misalignment effect suggested in (11), DoA accuracy improves significantly, reducing the RMSE by half to 6.0°, which validates the effectiveness of our calibration method in a realistic, challenging environment.

C. Comparison With Other RSS-Based DoA Methods: Computational Complexity

As established in Section II-A, conventional high-resolution DoA estimation methods, such as MUSIC and ESPRIT are computationally prohibitive for the resource-constrained IoT platforms targeted in this work. Fulfilling the design requirements for mobile tags—such as low power consumption and real-time capability—demands minimizing computational load to reduce response time and improve scalability. [35].

Our proposed method achieves this by minimizing computational burden through a simple RSS comparison. While magnitude-based methods, such as the monopulse technique [11], [29] offer simpler processes than CSI-based approaches, they still require multiple multiplication and division operations. In stark contrast, the proposed method's core operation is a single subtraction. This fundamental difference significantly reduces computational load, as empirically validated by our MATLAB simulations: the proposed method was 33% faster than the monopulse method (1.53 s versus 2.23 s) when estimating 100 incident angles.

To provide a broader comparative context, Table II summarizes the key differences between our method and other representative localization techniques across multiple dimensions, including theoretical complexity, core operations, and hardware requirements. As the table clearly illustrates, our approach combines the efficiency of an O(1) algorithm with minimal hardware demands, distinguishing it from the computationally intensive nature of MUSIC/ESPRIT and the complex hardware requirements of round trip time (RTT)-based systems. This streamlined, efficient design makes the proposed method uniquely suitable for scalable, real-time localization in compact mobile tag systems.

TABLE III
COMPARISON OF THE PROPOSED METHOD WITH RELATED WORK

	[10]	[35]	[27]	[37]	This Work
DoA Estimation Method	PPCC* Algorithm	Phase Difference Profile Calculation	Sum-Difference	Sum-Difference	Difference only
Frequency Band (GHz)	2.4	2.4	2.45	2.45	6.5
Normalized Physical Size (λ^3)	0.47	N/A	N/A	1.87	1
# of Antennas	12	8	1	2	2
FoV (°)	360	360	180	60	90
Validation Across Multiple Tag Distances	No	No	No	Yes	Yes
Estimation Error RMSE (°)	7.9	24.8	14**	5.89**	0.87***/ 6.0**

* PPCC: Power-Pattern Cross-Correlation
**Conducted outside the Anechoic Chamber
***Conducted in Anechoic Chamber

D. Comparison With Conventional RSS-Based DoA Systems

In Table III, the proposed method demonstrates advantages over other conventional RSS-based DoA estimation studies, offering enhanced accuracy. In this comparison, a tag with a 1 × 2 array tilted at 60° is used. In [10] and [35], a 360° FoV is achieved by using multiple sensors and active switches on the devices. However, the added active elements, circuits, and sensors increase the device's size, making it less suitable for mobile applications. Even with these complex additional components, the DoA estimation accuracy of the proposed work is four times higher than that of [35].

To achieve a more compact design, the device in [27] employs a single frequency-scanning antenna and a frequency-hopping scheme to extend the FoV without complex networks. This setup attains a 180° FoV with an RMSE estimation error of 14.3°. However, as noted, the authors validated the DoA estimation in an ideal scenario—at the same distance where the RSS was obtained—by varying the incident angle of the tag within an anechoic chamber. As indicated in [36], the ranging effect is inherent in RSS-based DoA estimation; therefore, incorporating range variation is essential for a comprehensive validation of proposed DoA methods. To address the ranging effect on DoA estimation, [37] calibrates the ranging effect based on the estimated range using RTT data, achieving an estimation error of 5.89°. Even with validation across different ranges from 0.5 to 3.0 m, the estimation error is significantly reduced compared to [27].

The proposed approach demonstrates stable performance across distances ranging from 1.8 to 4.5 m without requiring additional ranging calibration. This approach eliminates the

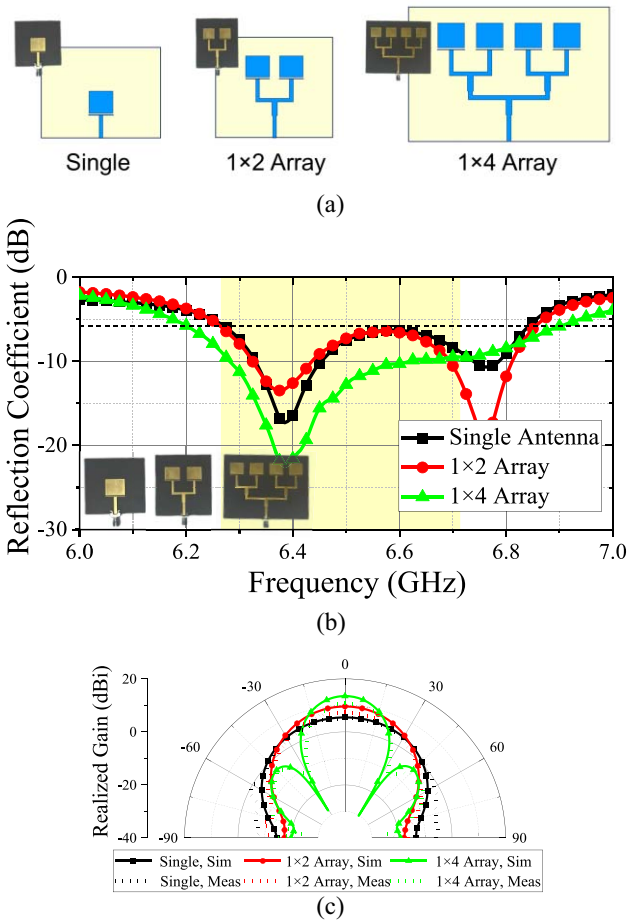

Fig. 11. (a) Three antenna types for the verification: Single, 1 × 2 array and 1 × 4 array antenna. (b) Reflection coefficients of three antennas. The yellow-shaded region represents UWB channel 5 band. (c) Simulated and Measured Radiation patterns of three antennas in the H-plane at 6.5 GHz.

need for additional processes, such as CSI and RTT calculations that require complex hardware structures, focusing instead on calibrating the misalignment effect between the tag and anchor. As a result, the proposed work achieves accuracy comparable to [37] while maintaining 1.5 times wider FoV. Utilizing localization determined by two or more reference points could offer a means of obtaining ranging information. This approach would allow for the incorporation of the ranging effect, as in [37], creating the potential to enhance both DoA and localization accuracy.

V. Tag Antenna Design Effect on DoA Performance

In Sections III and IV, we propose and validate an efficient DoA estimation method suitable for mobile tag devices in real-world scenarios. This section explores another critical aspect of implementing localization systems in resource-constrained tags—examining the relationship between parameterized tag design elements and DoA estimation performance. The impact of tag antenna design on DoA accuracy is analyzed, with a particular focus on antenna directivity as a key design factor. Antenna directivity is generally preferred to be high [29]. It can be improved by increasing the antenna's aperture size, though a larger antenna requires more physical space—which constrains integration of the tag into mobile devices. Finally, by incorporating tilting angle as a key design factor, the RSSD slope effectively integrates both major design parameters into a single performance metric. While directivity and tilting angle independently impact DoA performance, a unified metric that captures their combined effect is essential. The RSSD slope serves this role by quantifying the sensitivity of DoA estimation to variations in RSS. This novel metric provides a powerful tool that can be leveraged to optimize the tradeoff between hardware design constraints and localization performance.

TABLE IV
Radiation Characteristics of Three Antennas in Fig. 11

@ 6.5 GHz	Single	1×2 Array	1×4 Array
H-plane θ_{HPBW} (deg)	62	53	25
Directivity (dBi)	6.9	10.4	13.88
Radiation Efficiency (%)	66	50	51
Meas. Realized Gain (dBi)	5.12	7.45	10.96

A. Overview of Antenna Setup for Validation

To investigate the effect of tag design on DoA performance, three different antennas are utilized. Using printed circuit board (PCB) technology, as illustrated in Fig. 11(a), single, 1 × 2, and 1 × 4 array of patch antennas are designed on a TLY-5 substrate ($\epsilon_r = 2.2$) featuring a thickness of 0.76 mm By adjusting the number of antenna elements, the beamwidth and directivity of each antenna can be appropriately tailored as shown in Fig. 11.

To satisfy ultrawideband channel characteristics covering UWB channel 5 (f_c = 6489 MHz, BW = 499.2 MHz [38]), a quarter-wave line as a resonator from [39] is adopted. As shown in Fig. 11(b), the −6 dB reflection-coefficient bandwidths for the single, 1 × 2, and 1 × 4 patch antennas are 6.26–6.86 GHz, 6.26–6.86 GHz, and 6.20–6.89 GHz, respectively – fully covering the UWB channel 5 band in each case. The H-plane radiation pattern of each antenna is shown in Fig. 11(c). The solid lines show simulation results, while the dotted lines show measured results of each antenna. Table IV summarizes other key parameters for single, 1 × 2, and 1 × 4 patch arrays, including radiation efficiency, gain, directivity, and half-power beamwidth (HPBW). As the number of elements increases, antenna directivity improves, while the beamwidth narrows.

Additionally, a critical factor influencing DoA performance is the antenna's tilt angle. To thoroughly examine the effect of tilting angles in a tilted array configuration, nine distinct angles, ranging from 0° to 80° in 10° increments, are incorporated into the tag designs for numerical analysis, with three of these angles selected for experimental evaluation.

B. Numerical validation on DoA Estimation

A total of 27 tag designs are evaluated through theoretical analysis, with variations in antenna directivity across three types and tilting angles ranging from 0° to 80° in 10° increments. Several simulations are conducted using Ansys HFSS to derive the antenna radiation patterns shown in Fig. 11. Based on these patterns, we computed the expected RSSD(θ) curve and the corresponding RSSD$_m$ values for each tag design. The expected RSSD(θ) and measured RSSD$_m$ for different three tags—using different antennas but identical tilting angle, 40°—are represented in Fig. 12. The solid lines represent the predicted RSSD(θ) for three tags, with the black line for the single antenna, red for the 1 × 2 array, and green for the 1 × 4 array, which constitute the tag device. The scatter points represent the RSSD$_m$ used to evaluate the DoA estimation performance of the tag. The RSSD$_m$ data for tag evaluation are generated by incorporating random noise effects into the predicted RSSD(θ), as indicated in (14). Each RSS value is perturbed by a noise component $w_n$in (2), following a Gaussian distribution with the standard deviation σ_{RSS}

$$\text{RSS}_n^{\text{dB}} \sim N(G_n(\theta) + P(D), \sigma_{\text{RSS}}). \tag{14}$$

The scatter colors correspond to those of the predicted RSSD(θ), each derived from the same tag antenna.

In Fig. 12, it is clearly confirmed that three different tags have different RSSD slopes. The RSSD slope can be expressed as

$$\text{RSSD Slope} \triangleq \left| \frac{\text{RSSD}(\theta) - RSSD(\widehat{\theta})}{\theta - \widehat{\theta}} \right| \cong \left| \frac{RSSD(\theta) - RSSD_m}{\theta - \widehat{\theta}} \right| = \left| \frac{\Delta RSSD}{\Delta \theta} \right| \tag{15}$$

where θ represents the actual incident angle, $\widehat{\theta}$ the estimated incident angle, and $RSSD_m$ the measured RSSD value. According to (15), the RSSD slope is defined as the ratio of the difference in RSSD to a small angular variation at a specific incident angle. This angular variation can correspond to the estimation error. The estimated angle $\widehat{\theta}$ is determined using (7), where RSSD($\widehat{\theta}$) is adjusted to approximate RSSD$_m$ closely. Intuitively, a steeper RSSD slope acts as a gear ratio for angular estimation. It means that a large, easily measurable change in RSSD corresponds to a small change in angle. Consequently, any small, unavoidable error in RSSD measurement due to noise will be geared down into a much smaller, often negligible, error in the final angle estimation. This inherent noise resilience is why a higher RSSD slope directly leads to improved DoA accuracy.

Every tag design produces distinct average RSSD slopes using simulation and experimental data, as shown in Fig. 13(a). The average RSSD slope is defined as the ratio of the peak-to-peak RSSD value to the FoV size, which are primarily influenced by antenna directivity and tilting angle, respectively. In Fig. 13(a), the black, red, and green-filled scatter points represent the average RSSD slope for varying tilting angles, corresponding to the single antenna, 1 × 2 array, and 1 × 4 array antennas, respectively, based on simulation results. Notably, in the case of the 1 × 4 array antenna,

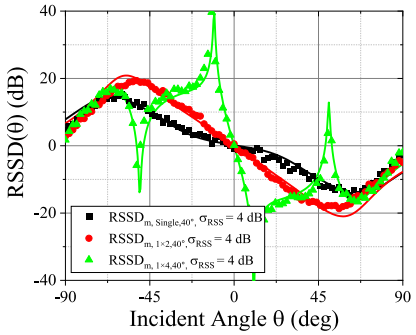

Fig. 12. Reference RSSD varying with the incident angle θ and processed RSSD$_m$ reflecting $\sigma_{\text{RSS}} = 4$ dB.

the RSSD slope reaches its maximum value at 60°. This occurs because, as the tilting angle approaches the first null beamwidth, the FoV narrows toward zero, thereby maximizing the average RSSD slope.

The RSSD slope is thus introduced as a robust metric for quantifying the impact of tag design on DoA estimation accuracy. Its validity is supported by two key observations: 1) each unique tag design yields a distinct and predictable RSSD slope and 2) the formal definition of the RSSD slope, as shown in (15), directly links RSSD variations to angular estimation errors, providing a clear theoretical basis for its use as a performance predictor. Furthermore, we validate the definition of the RSSD slope in terms of DoA accuracy under varying noise levels by adjusting the standard deviation (σ_{RSS}) of random noise—set at 2, 4, and 8 dB in (14). Fig. 13(b), the dashed lines in black, red, and green represent the DoA estimation accuracy for σ_{RSS} values of 2 dB, 4 dB, and 8 dB, respectively. The estimation accuracy is presented as RMSE within the limited FoV range of each tag device. The results demonstrate a consistent relationship between the averaged RSSD slope and DoA accuracy, highlighting an inversely proportional correlation under varying noise standard deviations, as indicated in (15). This result confirms the applicability of the RSSD slope as a reliable metric for tag design across different noise conditions.

C. Experimental Validation on DoA Accuracy

To experimentally validate the RSSD slope as a metric, nine selected tags are tested in an anechoic chamber, ensuring a consistent environment for fair evaluation. The experiments involve three different antenna configurations: 1) single; 2) 1 × 2 array; and 3) 1 × 4 array. In [29], a conventional monopulse radar design guide suggests setting the tilting angle to half of the HPBW when using a highly directional antenna. Following a monopulse radar design rule of thumb [29], we chose 10° for the 1 × 4 array and 40° for the 1 × 2 array. Additionally, we tested a 60° tilt since it maximizes the RSSD slope. The effect of tag design on DoA accuracy is evaluated through two approaches: 1) processed RSSD$_m$ under varying noise standard deviations and 2) the measured RSSD$_m$ from repeated measurements.

The overall experimental setup is illustrated schematically in Fig. 14. The tag and anchor are positioned at a distance of

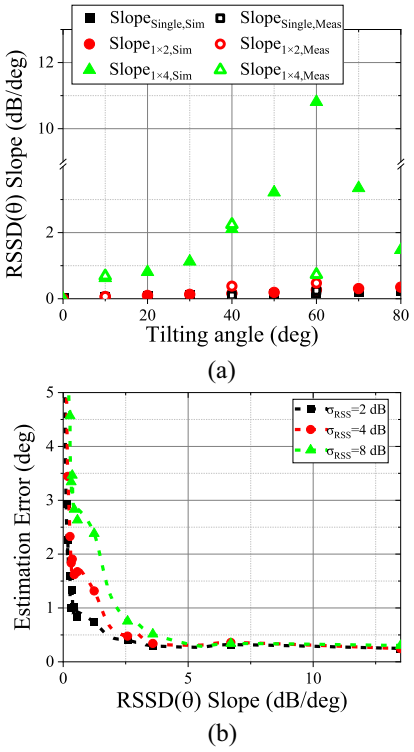

Fig. 13. (a) RSSD slope variation across different tag designs derived from Simulation and Measurement results. The black, red, and green scatter points correspond to tags using the single, 1 × 2, and 1 × 4 array antennas, respectively. (b) Relationship between RSSD slope and DoA Estimation errors under varying noise level using simulated results.

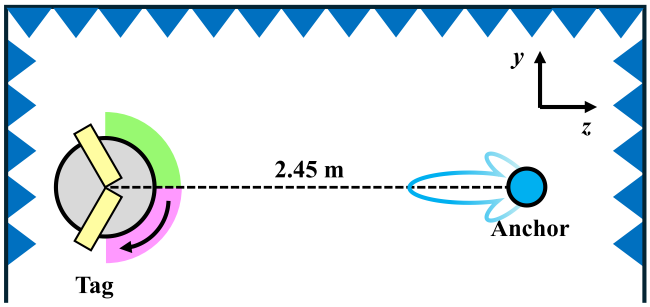

Fig. 14. Schematic of Experimental setup in Anechoic chamber.

2.45 m apart, adhering to far-field condition requirements. The RSS values are collected as the tag rotates in the *yz* plane from −60° to 60° in 1° increments. The transmitter sends 50 packets at each incident angle, and the receiver antenna collects 50 RSS values, using the average RSS. The incident angle is defined by comparing the tag's orientation to the anchor's.

Based on the measured RSS, reference RSSD(θ) in (6) for each tag is established. Post-processing is performed to establish a robust and high-resolution reference RSSD(θ) that resists environmental effects during measurements, incorporating techniques, such as smoothing and interpolation.

For experimental validation, the measured RSS from each antenna, as in the theoretical analysis, is used to derive processed RSSD$_m$ with varying σ_{RSS}. To verify the consistency of the RSSD slope under different channel conditions, σ_{RSS}

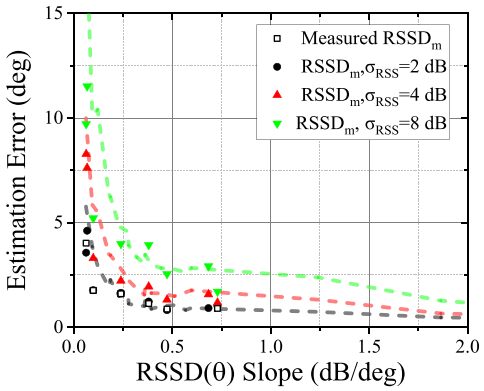

Fig. 15. Relationship between RSSD slope and DoA Estimation errors due to tag designs under measurement using measurement results.

TABLE V
RMSE BASED ON ANTENNA TYPES AND TILTING ANGLE IN THE MEASUREMENT RESULTS

RMSE		Antenna Types		
		Single	1×2 Array	1×4 Array
Tilting Angle	10°	4.02°	2.24°	1.06°
	40°	1.76°	1.13°	0.74°
	60°	1.60°	0.87°	0.90°

is varied at 2, 4, and 8 dB. The incident angle estimation is conducted according to (7), utilizing the post-processed RSSD(θ) and the synthetic RSSD$_m$ with varying σ_{RSS}. In Fig. 15, the colored scatter points represent the estimation error of the nine tested tags, with different colors indicating variations in σ_{RSS}. Similar to the simulation results for the 27 tags, represented by the lines, a higher RSSD slope in the colored scatter points corresponds to a lower estimation error, even under varying σ_{RSS}. In other words, the experimental results confirm the validity of the RSSD slope definition across different noise conditions.

Another approach to verification involves evaluating tag performance using repeated RSSD$_m$ measurements from the anechoic chamber. For each tag, four additional rounds of RSSD$_m$ measurements are conducted for evaluation, with the results compared against the reference RSSD. The DoA estimation results based on measured RSSD$_m$ are presented in Fig. 15 and Table V. The estimation accuracy is assessed by averaging the RMSE across the four rounds of RSSD$_m$ measurements. The results obtained from the actual measurement data, presented in Fig. 15, further validate the RSSD slope definition, confirming its inverse correlation with estimation error. Even though some discrepancies occur, such as an unexpectedly small RSSD slope for the tag with a 1 × 4 array antenna tilted at 60°— due to the receiver module's sensitivity limitations—the overall trend still follows the inverse relationship between RSSD slope and DoA accuracy.

Ultimately, balancing DoA estimation performance with the resource constraints of small handheld tag devices is a critical challenge. In this context, the proposed RSSD slope

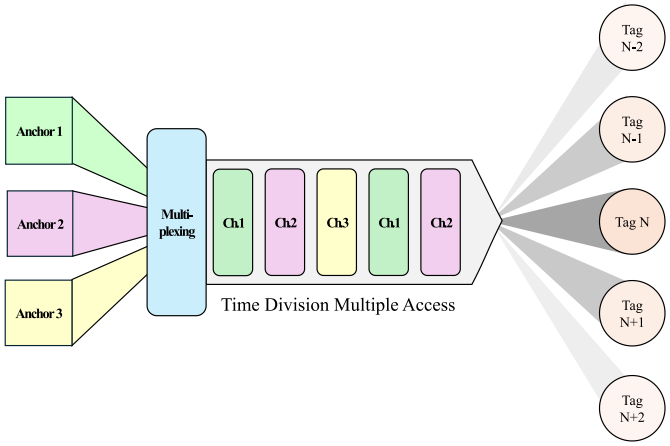

Fig. 16. Illustration of multianchor TDMA scheduling.

effectively captures the influence of tag antenna design on DoA accuracy and provides a simple yet robust quantitative metric for evaluating and optimizing tag designs early in the design phase, as demonstrated by the strong correlation between simulation and measurement results shown in Fig. 15. As discussed in Section II, not only DoA accuracy but also FoV—representing the angular region within which reliable DoA estimation is achievable—is a crucial performance metric in localization systems. The RSSD slope clearly reveals a fundamental tradeoff between angular sensitivity and FoV coverage. Accordingly, the representative tag design used for validating our calibration method was derived based on the RSSD slope metric, explicitly leveraging this sensitivity-FoV tradeoff to simultaneously optimize both DoA accuracy and effective FoV range for mobile handheld localization applications.

VI. Limitations and Future Work

Although we validated our core design in a controlled single-anchor, single-tag scenario, deploying the system in real-world IoT environments requires examining additional factors: scalability, robustness to environmental factors, and energy efficiency in real-time operation. This section discusses the system's limitations in these areas and outlines directions for future research.

A. Scalability in Multianchor Scenarios

Our framework's scalability stems from a deliberate design choice: an inverted, decentralized topology where anchors transmit and tags are passive receivers. This design fundamentally addresses the well-known scalability limitations of conventional centralized systems, in which a large number of tags transmit to a small set of anchors. In such traditional architectures, increasing the number of transmitting tags typically leads to medium access contention, increased synchronization overhead, and processing bottlenecks at the anchor nodes. In contrast, our approach eliminates these issues at the root by ensuring that tags do not initiate any transmissions and therefore do not compete for shared RF resources. As a result, the system maintains inherent scalability, allowing the number of tags to grow without imposing additional communication burden on the infrastructure.

While increasing the number of tags does not directly cause interference, since tags are passive, ultradense deployments can raise the ambient noise floor due to RF congestion and introduce adjacent-channel interference. These indirect physical-layer effects become significant limitations in very dense or noisy RF environments. By incorporating robust signal preprocessing and interference-aware scheduling mechanisms, these issues can be mitigated. Coordination among anchors can be achieved through conventional MAC-layer schemes, such as time-division multiple access [40], frequency-division multiple access [41], or code-division multiple access [42] to prevent signal collisions. As Fig. 16 illustrates, using a TDMA schedule with dedicated time slots for each anchor allows each anchor to transmit in turn. Here, a further advantage lies in the modularity of our DoA estimation algorithm, which operates independently for each anchor–tag pair. This enables a seamless extension to multianchor configurations without requiring any modification to the core estimation algorithm. The tag can then process each anchor's signal separately with the RSSD-based method. After obtaining incident angles from multiple anchors, standard localization techniques, such as triangulation or multilateration yield the tag's position. These characteristics collectively confirm that our decentralized architecture is not merely a theoretical construct but a practical and scalable framework ready for deployment in dense, real-world IoT environments.

B. Environmental Effect on RSSD

The efficacy of any RF localization system is inherently limited by the physical environment through which its signals propagate. In ideal free-space conditions, RF energy travels along a direct LoS path. In contrast, indoor environments create highly complex propagation scenarios where signals reflect off surfaces, diffract around obstacles, and scatter from small objects. The signal received at each antenna is thus a superposition of the LoS component and multiple multipath components, each arriving with different amplitudes and phases. This can lead to constructive or destructive interference and cause the RSS to fluctuate rapidly over small distances.

To evaluate the robustness of the proposed RSSD-based DoA estimation under such conditions, simulation studies were conducted using randomly distributed scatterers modeled in Ansys HFSS. In the simulated setup, as illustrated in Fig. 17, the anchor was placed at (0, 0, 1000) mm, and the tag with an interantenna spacing of 60 mm is positioned at the origin. Two scatterers, each of size 100 mm × 100 mm × 100 mm, were randomly placed within a defined spatial volume to emulate a moderately cluttered environment. The received RSS at nth antenna is modeled by the following expression:

$$\mathrm{RSS}_n = 10\log\left\{P_t\ G_{\mathrm{tx}}G_{rx,n}(\theta_{\mathrm{inc}})\left(\frac{C}{4\pi D_{rf}}\right)^2 + \sum_{k=1}^{P} G_{\mathrm{tx}}(\theta_{\mathrm{tilt}})G_{rx,n}\left(\theta_{\mathrm{inc},k}\right)\left(\frac{C}{4\pi D_{kf}}\right)^2 + w_n\right\}. \quad (16)$$

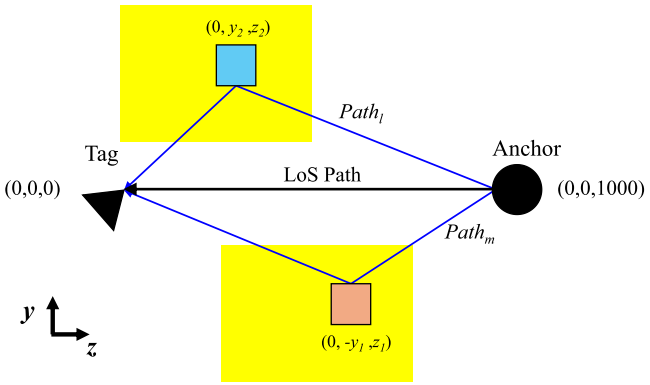

Fig. 17. Schematic of RSSD-based DoA method considering Multipath propagation. The yellow boxes indicate the available space for each scatterer.

This formulation consists of three components: 1) the gain as a function of the incident angle θ_{inc}; 2) interference from multipath components; and 3) additive noise. In scenarios where both tag antennas receive a dominant LoS component, the contributions from multipath and noise become negligible. Under this condition, the RSSD can be approximated solely by the antenna gain difference, which is directly related to the DoA

$$\begin{aligned}\text{RSSD} &= \text{RSS}_1 - \text{RSS}_2 \\ &= G_{\text{rx},1}(\theta_{\text{inc}}) - G_{\text{rx},2}(\theta_{\text{inc}}) + \text{Multipath} \quad \text{effect+n} \\ &\approx G_{\text{rx},1}(\theta_{\text{inc}}) - G_{\text{rx},2}(\theta_{\text{inc}}). \end{aligned} \tag{17}$$

The RSSD is inherently a combination of the ideal gain difference and error terms induced by multipath and noise. Our core hypothesis is that even in the presence of multipath, the error term is often minimized because multipath components affect both antennas in a correlated manner, leading to partial cancellation in the subtraction. Simulation results confirm this principle, with the mean DoA error remaining below 5°. This demonstrates the method's robustness in moderately cluttered environments where the LoS path is at least partially preserved. Nevertheless, in more challenging environments, particularly when one antenna experiences deep fading or complete signal blockage, the reliability of RSSD measurements degrades significantly. To enhance robustness in such cases, several mitigation strategies can be employed across different system levels:

1) System Level: In multianchor configurations, the localization process can dynamically select an alternative anchor [43] that maintains better visibility to both tag antennas. This adaptive anchor selection ensures that the most favorable signal paths are utilized, reducing the adverse effects of Non-LoS (NLoS) conditions and severe multipath interference.

2) Hardware Level: Robustness can be embedded into the tag design by employing advanced antenna architecture. Dual-polarized antennas, for example, leverage polarization diversity to better capture the LoS signal [44] while mitigating reflected signals which often have altered polarization.

3) Signal Processing Level: On platforms with higher computational capacity, advanced algorithms can move beyond simple mitigation and treat multipath components as structured, parametric interferences that can be surgically removed. By analyzing the received signal in the time–frequency domain, it becomes possible to isolate the dominant LoS path from multipath contamination. In particular [45], time–frequency analysis techniques, such as the Wigner–Hough transform (WHT), can be employed to extract the instantaneous frequency ridge associated with the LoS component on the time–frequency plane. Once the LoS trajectory is identified, adaptive filtering can be applied to suppress interfering components that deviate from it. These advanced signal processing methods collectively enable robust and accurate DoA estimation in densely multipath-rich RF environments.

While these methods add computational overhead, they provide a viable path to robust, accurate DoA estimation in challenging RF environments.

C. Energy Efficiency

Energy consumption in embedded systems is a critical design constraint shaped by the interaction among hardware characteristics, software operations, and system-level architecture [46], [47]. For battery-powered devices, the total energy budget is defined as the product of average power consumption (P_{avg}) and the total operational time (T_{total}). Therefore, minimizing P_{avg} is essential to prolong device lifetime. Many modern low-power systems adopt duty-cycled operation, where the system spends the majority of time in a deep sleep state and periodically wakes for brief intervals to perform essential tasks. Under this model, the average power consumption is given by

$$P_{\text{avg}} = \frac{P_{\text{active}} \cdot T_{\text{active}} + P_{\text{sleep}} \cdot T_{\text{sleep}}}{T_{\text{active}} + T_{\text{sleep}}}. \tag{18}$$

The proposed RSSD-based DoA estimation method aligns well with this low-power paradigm [48], as it is inherently energy- efficient due to its minimal computational requirements. Specifically, the core operation consists of a single subtraction between two RSS values—an extremely lightweight instruction on typical embedded processors, such as those in the ARM Cortex-M family. Traditional high-resolution AoA techniques, such as MUSIC and ESPRIT, require computationally intensive tasks, including covariance matrix formation, eigenvalue decomposition, and spectral scanning. By contrast, our method's simple single-subtraction operation substantially reduces both the active power (P_{active}) and active duration (T_{active}). This enables the device to return to its low-power sleep mode almost immediately after completing a measurement.

A significant source of energy inefficiency in duty-cycled wireless systems is idle listening, during which the radio front-end remains powered while waiting for potential transmissions. To mitigate this, our framework can be augmented with Wake-up Radio (WuR) technology [49]. A WuR is an auxiliary ultralow-power receiver on the order of microwatt consumption that continuously monitors the channel and triggers the main UWB radio upon detecting a specific wake-up signal. This mechanism effectively eliminates idle listening, allowing the primary transceiver to remain in deep sleep until

TABLE VI
ESTIMATION ERROR VARIATIONS ACROSS AVERAGING WINDOW SIZE

Averaging Window Size	5	10	15	30	60
Estimation Error (°)	1.72	1.31	1.05	0.77	0.68

needed. Integrating WuR with UWB systems is an active area of research, with the potential to enable ultralow-power localization solutions.

D. Real-Time Operation

In dynamic scenarios, the required update frequency is fundamentally determined by the angular velocity of the moving tag. If the tag moves with a linear velocity v_1 at a radial distance R from the anchor, the instantaneous angular velocity can be expressed as $\omega = v_1/R$. To achieve a directional resolution of 1°, the system must update at a rate higher than $\omega/(1°)$. For example, with $v_1 = 5$ m/s and $R = 10$ m, the angular velocity is 0.5 rad/s $\approx 28.6°$ /s, which requires an update rate exceeding 28 Hz. Under such conditions, the averaging window size must be shortened to meet the latency requirement.

Table VI summarizes the relationship between the number of packets averaged and the resulting DoA accuracy. Reducing the averaging window from 60 to 10 packets increases the RMSE from 0.68° to 1.31°, while even with as few as five packets, the RMSE remains below 2°. These results highlight a tradeoff between accuracy and responsiveness: shorter averaging enables rapid updates suitable for fast-moving targets, while still maintaining sub-2° estimation accuracy. Therefore, the tradeoff can be flexibly adjusted depending on application requirements, such as latency, mobility speed, and power constraints.

The proposed method is highly suitable for real-time implementation due to its exceptionally low computational complexity. In a prototype developed on an Arduino platform, the system was able to retrieve RSS values at a rate of approximately one packet per second. This update rate was not limited by the algorithm itself, but rather by hardware constraints—specifically, the data transfer speed of the SPI and serial communication interfaces on the microcontroller. In practical embedded environments, the achievable update frequency is primarily determined by the rate at which the UWB transceiver can acquire and report RSS measurements. Fortunately, UWB radios inherently support high data rates and low latency, enabling the acquisition of significantly more packets within a single update interval. This capability enables the use of sufficiently large averaging windows without sacrificing update frequency, thereby improving accuracy while preserving responsiveness. Consequently, unlike matrix-based or machine learning-based DoA estimators where computational complexity is the primary bottleneck, the proposed RSSD-based method is inherently lightweight, with its performance ceiling dictated by radio hardware throughput rather than algorithmic complexity. This firmly confirms its suitability for real-time deployment on resource-constrained platforms.

VII. CONCLUSION

This article has presented and validated a novel dual-pronged tag system for small, battery-powered devices, successfully addressing the critical challenges of computational complexity, hardware design optimization, and estimation accuracy in real-world scenarios. The proposed RSSD-based DoA estimation method reduces the core computation to a single subtraction, ensuring seamless integration into resource-constrained devices. Critically, the framework effectively compensates for anchor-tag misalignment, halving the DoA estimation error from 12.5° to 6.0° across various tag distances (1.8 to 4.5 m).

Furthermore, this study tackles the practical challenges of antenna design by introducing the RSSD slope as a novel metric. This metric quantifies the intricate relationship between tag design and DoA. Experimental results confirm that a higher RSSD slope directly corresponds to a lower estimation error. The tag antenna, optimized using the RSSD-slope metric, acts in concert with the single-subtraction lightweight calibration algorithm. Together, they achieve an ultralow-complexity hardware–software synergy that cuts DoA error in half. This effectively bridges the gap between the software algorithm and the hardware design, solidifying the holistic nature of our dual-pronged approach. While the core framework demonstrates significant accuracy and efficiency, its future potential lies in its extensibility. The decentralized, passive-tag architecture is inherently scalable, and the DoA estimation module can be readily integrated into multianchor systems using standard protocols, such as TDMA to achieve full 2-D/3-D localization. The system also exhibits notable robustness in moderately cluttered environments. Future work can further enhance this resilience in severe NLoS conditions by employing adaptive anchor selection or advanced dual-polarized antennas. Moreover, the algorithm's ultralow computational complexity not only enables real-time performance but also creates a clear path toward near-zero-power operation through integration with emerging technologies, such as WuR. By synergistically reducing computational complexity, optimizing antenna design, and enhancing DoA accuracy, this work provides a comprehensive blueprint for developing the next generation of small, power-efficient, and scalable tag devices suitable for robust, real-world decentralized localization.

ACKNOWLEDGMENT

The authors thank Dongwoo FineChem, Korea for their support and in particular Dr. Dongpil Park.

REFERENCES

[1] F. Zafari, A. Gkelias, and K. K. Leung, "A survey of indoor localization systems and technologies," *IEEE Commun. Surveys Tuts.*, vol. 21, no. 3, pp. 2568–2599, 3rd Quart., 2019.
[2] Y. Li et al., "Toward location-enabled IoT (LE-IoT): IoT positioning techniques, error sources, and error mitigation," *IEEE Internet Things J.*, vol. 8, no. 6, pp. 4035–4062, Mar. 2021.
[3] E. H. Houssein, M. A. Othman, W. M. Mohamed, and M. Younan, "Internet of Things in smart cities: Comprehensive review, open issues and challenges," *IEEE Internet Things J.*, vol. 11, no. 9, pp. 16845–16858, May 2024, doi: 10.1109/JIOT.2024.3449753.
[4] M. Elsanhoury et al., "Precision positioning for smart logistics using ultra-wideband technology-based indoor navigation: A review," *IEEE Access*, vol. 10, pp. 44413–44445, 2022.

[5] Z. He, M. Petovello, and G. Lachapelle, "Indoor Doppler error characterization for high sensitivity GNSS receivers," *IEEE Trans. Aerosp. Electron. Syst.*, vol. 50, no. 3, pp. 2354–2360, Jul. 2014.

[6] Y. Li, Y. Zhuang, P. Zhang, H. Lan, X. Niu, and N. El-Sheimy, "An improved inertial/wifi/magnetic fusion structure for indoor navigation," *Inf. Fusion*, vol. 34, pp. 101–119, Mar. 2017.

[7] T. Janssen, M. Weyn, and R. Berkvens, "Localization in low power wide area networks using Wi-Fi fingerprints," *Appl. Sci.*, vol. 7, no. 9, p. 936, Sep. 2017.

[8] S. Leugner, M. Pelka, and H. Hellbrück, "Comparison of wired and wireless synchronization with clock drift compensation suited for U-TDoA localization," in *Proc. 13th Workshop Position., Navig. Commun. (WPNC)*, Bremen, Germany, Oct. 2016, pp. 1–4.

[9] A. Cidronali, S. Maddio, G. Giorgetti, and G. Manes, "Analysis and performance of a smart antenna for 2.45-GHz single-anchor indoor positioning," *IEEE Trans. Microw. Theory Techn.*, vol. 58, no. 1, pp. 21–31, Jan. 2010.

[10] M. Groth, M. Rzymowski, K. Nyka, and L. Kulas, "ESPAR antenna-based WSN node with DoA estimation capability," *IEEE Access*, vol. 8, pp. 91435–91447, 2020.

[11] J. L. Gómez-Tornero, D. Cañete-Rebenaque, J. A. López-Pastor, and A. S. Martínez-Sala, "Hybrid analog-digital processing system for amplitude-monopulse RSSI-based MIMO WiFi direction-of-arrival estimation," *IEEE J. Sel. Topics Signal Process.*, vol. 12, no. 3, pp. 529–540, Jun. 2018.

[12] M. Qi, B. Xue, and W. Wang, "Calibration and compensation of anchor positions for UWB indoor localization," *IEEE Sensors J.*, vol. 24, no. 1, pp. 689–699, Jan. 2024.

[13] P. Krapež and M. Munih, "Anchor calibration for real-time-measurement localization systems," *IEEE Trans. Instrum. Meas.*, vol. 69, no. 12, pp. 9907–9917, Dec. 2020.

[14] M. Tarkowski and L. Kulas, "RSS-based DoA estimation for ESPAR antennas using support vector machine," *IEEE Antennas Wireless Propag. Lett.*, vol. 18, no. 4, pp. 561–565, Apr. 2019.

[15] Z. Kasmi, N. Guerchali, A. Norrdine, and J. H. Schiller, "Algorithms and position optimization for a decentralized localization platform based on resource-constrained devices," *IEEE Trans. Mobile Comput.*, vol. 18, no. 8, pp. 1731–1744, Aug. 2019.

[16] D. Chiasson, Y. Lin, M. Kok, and P. B. Shull, "Asynchronous hyperbolic UWB source-localization and self-localization for indoor tracking and navigation," *IEEE Internet Things J.*, vol. 10, no. 13, pp. 11655–11668, Jul. 2023.

[17] E. Gentilho, Jr., P. R. Scalassara, and T. Abrão, "Direction-of-arrival estimation methods: A performance-complexity tradeoff perspective," *J. Signal Process. Syst.*, vol. 92, no. 2, pp. 239–256, Feb. 2020.

[18] C. Stoeckle, J. Munir, A. Mezghani, and J. A. Nossek, "DoA estimation performance and computational complexity of subspace-and compressed sensing-based methods," in *Proc. 19th Int. ITG Workshop Smart Antennas (WSA)*, Ilmenau, Germany, Mar. 2015, pp. 1–6.

[19] N. BniLam, D. Joosens, J. Steckel, and M. Weyn, "Low cost AoA unit for IoT applications," in *Proc. 13th Eur. Conf. Antennas Propag. (EuCAP)*, Kraków, Poland, 2019, pp. 1–5.

[20] B. J. Dil and P. J. Havinga, "RSS-based localization with different antenna orientations," in *Proc. Aust. Telecommun. Netw. Appl. Conf.*, Auckland, New Zealand, 2010, pp. 13–18.

[21] P. Stoica and A. Nehorai, "MUSIC, maximum likelihood, and Cramer-Rao bound," *IEEE Trans. Acoust., Speech, Signal Process.*, vol. 37, no. 5, pp. 720–741, May 1989.

[22] R. Pöhlmann, S. Zhang, E. Staudinger, A. Dammann, and P. A. Hoeher, "Simultaneous localization and calibration for cooperative radio navigation," *IEEE Trans. Wireless Commun.*, vol. 21, no. 8, pp. 6195–6210, Aug. 2022.

[23] O. Jean and A. J. Weiss, "Geolocation by direction of arrival using arrays with unknown orientation," *IEEE Trans. Signal Process.*, vol. 62, no. 12, pp. 3135–3142, Jun. 2014.

[24] S.-Y. Huang and R.-B. Wu, "Positioning for search and rescue in GPS-denied area by distributed WiFi RSS-based DoA modules," *IEEE Access*, vol. 10, pp. 76105–76113, 2022.

[25] A. Zandamela, A. Chiumento, N. Marchetti, and A. Narbudowicz, "Angle of arrival estimation via small IoT devices: Miniaturized arrays vs. MIMO antennas," *IEEE Internet Things Mag.*, vol. 5, no. 2, pp. 146–152, Jun. 2022.

[26] D. Patron, H. Paaso, A. Mämmelä, D. Piazza, and K. R. Dandekar, "Improved design of a CRLH leaky-wave antenna and its application for DoA estimation," in *Proc. IEEE-APS Topical Conf. Antennas Propag. Wireless Commun. (APWC)*, Torino, Italy, Sep. 2013, pp. 1343–1346.

[27] A. Gil-Martínez, M. Poveda-García, J. A. López-Pastor, J. C. Sánchez-Aarnoutse, and J. L. Gómez-Tornero, "Wi-Fi direction finding with frequency-scanned antenna and channel-hopping scheme," *IEEE Sensors J.*, vol. 22, no. 6, pp. 5210–5222, Mar. 2022.

[28] L. J. Chu, "Physical limitations of omni-directional antennas," *J. Appl. Phys.*, vol. 19, no. 12, pp. 1163–1175, Dec. 1948.

[29] S. M. Sherman and D. K. Barton, *Monopulse Principles and Techniques*, 3rd ed. Norwood, MA, USA: Artech House, 2011.

[30] S. Han and B.-J. Jang, "Drone's angle-of-arrival estimation using a switched-beam antenna and single-channel receiver," *Sensors*, vol. 25, no. 8, p. 2376, Apr. 2025.

[31] A. Yassin et al., "Recent advances in indoor localization: A survey on theoretical approaches and applications," *IEEE Commun. Surveys Tuts.*, vol. 19, no. 2, pp. 1327–1346, 2nd Quart., 2017.

[32] S. Maddio, A. Cidronali, M. Passafiume, G. Collodi, M. Lucarelli, and S. Maurri, "Multipath robust azimuthal direction of arrival estimation in dual-band 2.45–5.2 GHz networks," *IEEE Trans. Microw. Theory Techn.*, vol. 65, no. 11, pp. 4438–4449, Nov. 2017.

[33] G. F. Hamberger, J.-A. Antón, S. J. Lachner, and B. Derat, "Correction of over-the-air transmit and receive wireless device performance errors due to displaced antenna positions in the measurement coordinate system," *IEEE Trans. Antennas Propag.*, vol. 68, no. 11, pp. 7549–7554, Nov. 2020.

[34] *DWM1000 Datasheet, Version 2.15*, Qorvo, Hillsboro, OR, USA, 2020.

[35] N. Paulino and L. M. Pessoa, "Self-localization via circular Bluetooth 5.1 antenna array receiver," *IEEE Access*, vol. 11, pp. 365–395, 2023.

[36] J. A. López-Pastor, A. Gómez-Alcaraz, D. Cañete-Rebenaque, A. S. Martinez-Sala, and J. L. Gómez-Tornero, "Near-field monopulse DoA estimation for angle-sensitive proximity WiFi readers," *IEEE Access*, vol. 7, pp. 88450–88460, 2019.

[37] J. A. López-Pastor, P. Arques-Lara, J. J. Franco-Peñaranda, A. J. García-Sánchez, and J. L. Gómez-Tornero, "Wi-Fi RTT-based active monopulse RADAR for single access point localization," *IEEE Access*, vol. 9, pp. 34755–34766, 2021.

[38] "First report and order, revision of part 15 of the commission's rules regarding ultra-wideband transmission systems," Fed. Commun. Comm., Washington, DC, USA, Rep. ET-Docket 98-153, FCC 02-48, Apr. 2002.

[39] J.-D. Zhang, L. Zhu, Q.-S. Wu, N.-W. Liu, and W. Wu, "A compact microstrip-fed patch antenna with enhanced bandwidth and harmonic suppression," *IEEE Trans. Antennas Propag.*, vol. 64, no. 12, pp. 5030–5037, Dec. 2016.

[40] Y. Cao, C. Chen, D. St-Onge, and G. Beltrame, "Distributed TDMA for mobile UWB network localization," *IEEE Internet Things J.*, vol. 8, no. 17, pp. 13449–13464, Sep. 2021.

[41] Z. Chen, Z. Zhang, Z. Xiao, Z. Yang, and R. Jin, "Deep learning-based multi-user positioning in wireless FDMA cellular networks," *IEEE J. Sel. Areas Commun.*, vol. 41, no. 12, pp. 3848–3862, Dec. 2023.

[42] S. De Lausnay, L. De Strycker, J.-P. Goemaere, N. Stevens, and B. Nauwelaers, "Optical CDMA codes for an indoor localization system using VLC," in *Proc. 3rd Int. Workshop Opt. Wireless Commun. (IWOW)*, Funchal, Portugal, Sep. 2014, pp. 50–54.

[43] M. Kolakowski, "Adaptive anchor pairs selection in a TDOA-based system through robot localization error minimization," in *Proc. Signal Process. Symp. (SPSympo)*, Lodz, Poland, Sep. 2021, pp. 128–132.

[44] M. B. Zid, K. Raoof, and A. Bouallegue, "Dual polarized versus single polarized MIMO: A study over NLOS propagation with polarization discrimination and spatial correlation effects," in *Proc. 6th Eur. Conf. Antennas Propag. (EUCAP)*, 2012, pp. 1979–1983.

[45] S. Barbarossa and A. Scaglione, "Adaptive time-varying cancellation of wideband interferences in spread-spectrum communications based on time-frequency distributions," *IEEE Trans. Signal Process.*, vol. 47, no. 4, pp. 957–965, Apr. 1999.

[46] H. Jayakumar et al., "Energy-efficient system design for IoT devices," in *Proc. 21st Asia South Pacific Des. Autom. Conf. (ASP-DAC)*, Macao, China, Jan. 2016, pp. 298–301.

[47] Z. Almudayni, B. Soh, H. Samra, and A. Li, "Energy inefficiency in IoT networks: Causes, impact, and a strategic framework for sustainable optimisation," *Electronics*, vol. 14, no. 1, p. 159, Jan. 2025.

[48] F. Yaghoubi, A.-A. Abbasfar, and B. Maham, "Energy-efficient RSSI-based localization for wireless sensor networks," *IEEE Commun. Lett.*, vol. 18, no. 6, pp. 973–976, Jun. 2014.

[49] R. Piyare, A. L. Murphy, C. Kiraly, P. Tosato, and D. Brunelli, "Ultra low power wake-up radios: A hardware and networking survey," *IEEE Commun. Surveys Tuts.*, vol. 19, no. 4, pp. 2117–2157, 4th Quart., 2017.

Myoungsun Kim (Graduate Student Member, IEEE) received the B.S. (summa cum laude) degree in electronic engineering from Soongsil University, Seoul, Republic of Korea, in 2021, and the M.S. degree in electrical engineering from Pohang University of Science and Technology, Pohang, Republic of Korea, in 2023, where she is currently pursuing the Ph.D. degree with the Department of Electrical Engineering under the supervision of Prof. W. Hong.

Her research interests include ultrawideband-based indoor localization, antenna-on-display technologies and leaky-wave antennas for next-generation wireless systems.

Ms. Kim has received the Mojgan Daneshmand Grant for the 2024 IEEE APS/URSI Symposium.

Sirous Bahrami (Senior Member, IEEE) received the B.S. degree from Isfahan University, Isfahan, Iran, in 2007, and the M.S. and Ph.D. degrees in electrical engineering from Iran University of Science and Technology, Tehran, Iran, in 2009 and 2014, respectively.

From 2014 to 2020, he was with the Department of Electrical Engineering, Salman Farsi University of Kazerun, Kazerun, Iran. He joined as a Postdoctoral Researcher with Pohang University of Science and Technology, Pohang, Republic of Korea, in 2021, where he is currently a Research Assistant Professor, developing multifeed and reconfigurable antennas for RF, and mm-wave communication systems. His research interests include passive and active microwave devices, planar antennas, and monolithic microwave integrated circuits.

Dr. Bahrami was a recipient of the Best Paper Award at the 2024 Electromagnetic Measurement Technology Conference, South Korea, the Best Student Paper Award Finalist at IEEE RFIC 2023, the Top Reviewers Award from IEEE TAP in 2024, the First Prize for Best Antenna Measurement Paper at ISAP 2024, the Excellence Paper Award at the 2025 Korean Electromagnetic Conference, and the Finalist in the IMS 2025 Early Career Paper Competition. He also received the Get Started Funding 2025 Program Grant from Lund University to support his research activities.

Wonbin Hong (Fellow, IEEE) is currently a Chaired Professor with Pohang University of Science and Technology (POSTECH), Pohang, South Korea. He is also the Co-Founder and the Co-CEO of Kreemo Inc. He is one of the first researchers to pioneer the concept and design of millimeter-wave antennas and RF front ends for cellular antenna-in-package in the field of consumer electronics, including mobile terminals and access points for the much-anticipated ultrafast broadband wireless solutions, such as 5G/6G and SATCOM. He is also the Inventor of Antenna-on-Display Technology. He has authored and co-authored more than 250 peer-reviewed journals, conference papers, and two book chapters and one book. He is the Inventor of more than 110 granted and 250 pending patents. He has been involved in more than 80 government and industry research projects and currently serves as a technical consultant to numerous multinational tech firms and government agencies.

Prof. Hong's students have received recognition, including the Student Best Paper Award during 2024 IEEE European Conference on Antennas and Propagation, the 1st Prize Best Industry Paper, and the 1st Prize Best Antenna Measurement Paper during 2024 International Symposium on Antennas and Propagation, the First Prize Best Student Paper Award, the Second Prize Best Paper Award during 2023 IEEE International Workshop on Antenna Technologies, the Second Place Best Student Paper Award in the 2021 IEEE AP-S Symposium on Antennas and Propagation, the First Place Best Student Paper Award in the 2020 IEEE AP-S Symposium on Antennas and Propagation, the Best Student Paper Award IEEE European Conference on Antennas and Propagation 2020, the First Prize Best Student Paper Award in 2018 International Symposium on Antennas and Propagation, and the Best Paper Award in 2017 ISMOT, the 2021 IT Award to the most Outstanding Doctorate Student of POSTECH, the 2022, 2020, 2018 Outstanding Master's Student, Electrical Engineering Department of POSTECH, the Gold Prize Award in 2023 Samsung Humantech Paper Award, the Silver Medal in the 14th Samsung ElectroMechanics Best Paper Award 2018. He is a member of the Young Korea Academy of Science and Technology and recipient of the 29th Young Engineer Award from the National Academy of Korea.